Thermodynamic and Kinetic Data for Adduct Formation, *cis–trans* Isomerization and Redox Reactions of ML_4 Complexes: A Case study with Rhodium– and Iridium–tropp Complexes in d^8, d^9 and d^{10} Valence Electron Configurations (tropp = Dibenzotropylidene Phosphanes)

Frank Breher,[a] Heinz Rüegger,[a] Marina Mlakar,[b] Manfred Rudolph,[c] Stephan Deblon,[a] Hartmut Schönberg,[a] Souad Boulmaâz,[a] Jörg Thomaier,[a] and Hansjörg Grützmacher*[a]

Dedicated to Prof. Dr. H. Werner on the occasion of his 70th birthday

Abstract: The formation of adducts of the square-planar 16-electron complexes *trans*-$[M(tropp^{ph})_2]^+$ and *cis*-$[M(tropp^{ph})_2]^+$ (M = Rh, Ir; $tropp^{Ph}$ = 5-diphenylphosphanyldibenzo[a,d]cycloheptene) with acetonitrile (acn) and Cl^-, and the redox chemistry of these complexes was investigated by various physical methods (NMR and UV-visible spectroscopy, square-wave voltammetry), in order to obtain some fundamental thermodynamic and kinetic data for these systems. A *trans*/*cis* isomerization cannot be detected for $[M(tropp^{ph})_2]^+$ in non-coordinating solvents. However, both isomers are connected through equilibria of the type *trans*-$[M(tropp^{ph})_2]^+ + L \rightleftarrows [ML(tropp^{ph})_2]^n \rightleftarrows$ *cis*-$[M(tropp^{ph})_2]^+ + L$, involving five-coordinate intermediates $[ML(tropp^{ph})_2]^n$ (L = acn, $n = +1$; L = Cl^-, $n = 0$). Values for K_d (K_f), that is, the dissociation (formation) equilibrium constant, and k_d (k_f), that is, the dissociation (formation) rate constant, were obtained. The formation reactions are fast, especially with the *trans* isomers ($k_f > 1 \times 10^5\,M^{-1}s^{-1}$). The reaction with the sterically more hindered *cis* isomers is at least one order of magnitude slower. The stability of the five-coordinate complexes $[ML(tropp^{ph})_2]^n$ increases with Ir > Rh and $Cl^- >$ acn. The dissociation reaction has a pronounced influence on the square-wave (SW) voltammograms of *trans*/*cis*-$[Ir(tropp^{ph})_2]^+$. With the help of the thermodynamic and kinetic data independently determined by other physical means, these reactions could be simulated and allowed the setting up of a reaction sequence. Examination of the data obtained showed that the *trans*/*cis* isomerization is a process with a low activation barrier for the four-coordinate 17-electron complexes $[M(tropp^{ph})_2]^0$ and especially that a disproportionation reaction 2 *trans*/*cis*-$[M(tropp^{ph})_2]^0 \rightarrow [M(tropp^{ph})_2]^+ + [M(tropp^{ph})_2]^-$ may be sufficiently fast to mask the true reactivity of the paramagnetic species, which are probably less reactive than their diamagnetic equilibrium partners.

Keywords: cyclic voltammetry · iridium · mechanisms · phosphanes · rhodium

Introduction

The syntheses of stable paramagnetic rhodium and iridium complexes in their formal oxidation state (0) have been reported recently.[1–5] Such d^9 valence-electron-configured complexes were not explored in depth previously. In addition, much of the chemistry of d^{10}-configured rhodate and iridate complexes remains to be investigated, even though these electron-rich compounds have been known for about 35 years.[6–12] These four-coordinate 17-electron and 18-electron complexes merit attention, because they have promising potential in bond activation chemistry[13–16] and have been discussed in the context of the photocatalytic H_2O[17] and HBr[18] splitting.

[a] Dr. F. Breher, Dr. H. Rüegger, Dr. S. Deblon, Dr. H. Schönberg, Dr. S. Boulmaâz, Dr. J. Thomaier, Prof. H. Grützmacher
Department of Chemistry and Applied Biology (D-CHAB)
ETH Hönggerberg, Wolfgang-Pauli Str.
8093 Zürich (Switzerland)
Fax: (+41) 1-633-10-32
E-mail: gruetzmacher@inorg.chem.ethz.ch

[b] Dr. M. Mlakar
Center for Marine Research-Zagreb
Rudjer Bošković Institute, Bijenička 54
10001 Zagreb (Croatia)

[c] Dr. M. Rudolph
Faculty of Chemistry
Friedrich-Schiller-University of Jena
August Bebel Str. 2, 07743 Jena (Germany)

 DOI: 10.1002/chem.200305116

The ligand systems used to date for the preparation and isolation of stable M^0 complexes are 1) 5-diphenylphosphanyl-dibenzo[a,d]cycloheptene (dibenzotropylidene phosphines = tropp^{ph}),[1,2] 2) 1,1′-bis(diphenylphosphino)ferrocene (dppf),[3,4] and 3) 3,3′,4,4′-tetramethylbiphosphinine (tmbp).[5]. Although electronically quite different, they have a rigid bidentate metal binding site in common.

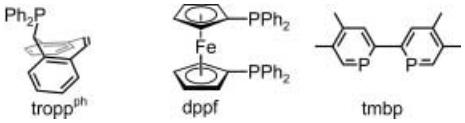

In previous work[1,2,19] we showed that the 16-electron $[M(tropp^{ph})_2]^+$ complexes **1**-M (M = Rh, Ir) are reversibly reduced at remarkable low negative potentials in two consecutive one-electron transfer steps, to give the neutral paramagnetic 17-electron $[M(tropp^{ph})_2]^0$ **2**-M (M = Rh, Ir), and the 18-electron ate-complexes $[M(tropp^{ph})_2]^-$ **3**-M (M = Rh, Ir). For M = Ir, we investigated various reactions of the complexes **1**-Ir, **2**-Ir, and **3**-Ir, which have different valence electron configurations, with protic reagents or dihydrogen.[20]

As a result, we obtained the simplified reaction diagram shown in Scheme 1, in which two electrons (steps a and b)

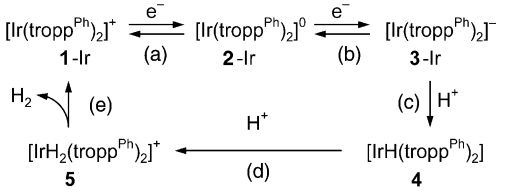

Scheme 1. Simplified cycle for H_2 production with iridium tropp complexes.

and subsequently two protons (steps c and d) are added "dropwise", to finally produce dihydrogen (step e).[21] Reaction e proceeds at room temperature and is remarkable clean. This cycle includes all chemical steps that are necessary to produce dihydrogen from proton sources by using a single site catalyst. Note that all complexes shown in Scheme 1 were isolated and fully structurally characterized.

A key-point for the rational design of such cycles is a better knowledge of the thermodynamic and kinetic parameters which interconnect the participating species. At this point, an evaluation of the reactivity of the 17-electron complex $[Ir(tropp^{ph})_2]^0$ (**2**-Ir) was of special interest. We investigated the reaction of **2**-Ir with H_2 or protons and observed, in both cases, the quantitative formation of the very stable 18-electron monohydride complex $[IrH(tropp^{ph})_2]$ (**4**). However, the 16-electron complexes *trans/cis*-$[Ir(tropp^{Ph})_2]^+$ (*trans*/*cis*-**1**-Ir) and the 18-electron iridate $[Ir(tropp^{Ph})_2]^-$ (**3**-Ir) also react rapidly and exothermically with H_2 to yield either the octahedral cationic iridium(III) dihydride $[IrH_2(tropp^{ph})_2]^+$ (**5**), which is stable under an atmosphere of H_2, or the monhydride **4**, respectively.[20] Thus it is possible that the "reactivity" of the 17-electron complexes *trans/cis*-$[Ir(tropp^{Ph})_2]^0$ (**2**-Ir) is evoked in reality by the diamagnetic closed-shell species *trans/cis*-**1**-Ir and **3**-Ir, which may be present in the equilibrium given in Equation (1), which is characterized by the disproportionation constant K_{disp}.

$$2\,trans/cis\text{-}[Ir(tropp^{Ph})_2]^0 \rightleftharpoons trans/cis\text{-}[Ir(tropp^{Ph})_2]^+ + [Ir(tropp^{Ph})_2]^- \quad (1)$$

We show in this paper that a satisfactory answer to this question can be found by digital simulation of electrochemical data of a redox system that also includes non-redox equilibria. Some of these data were determined independently by other physical means. The paper is divided into two parts. In the first part, we investigate the structures and simple addition reactions of the four-coordinate 16-electron complexes $[M(tropp^{ph})_2]^+$ (M = Rh, Ir) with donor ligands such as tetrahydrofuran (thf), acetonitrile (acn), or chloride by NMR techniques. In the second part we discuss the electrochemistry of the iridium complex $[Ir(tropp^{ph})_2]^+$ (**1**-Ir).

Results

Molecular structures of $[Rh(acn)(tropp^{ph})_2]^+PF_6^-$ (6-Rh) and $[IrCl(tropp^{ph})_2]$ (7-Ir). As this study is concerned with the formation and dynamics of five-coordinate rhodium– and iridum–bis(tropp) complexes, we first discuss briefly the structures of $[Rh(acn)(tropp^{Ph})_2]^+$ (**6**-Rh) (acn = acetonitrile) and $[IrCl(tropp^{Ph})_2]$ (**7**-Ir). Crystallization of the four-coordinate complex *trans/cis*-$[Rh(tropp^{ph})_2]^+PF_6^-$ (**1**-Rh) from a concentrated solution in acetonitrile gave a mixture of red and a few yellow crystals. The red ones contain the *trans* isomer of **1**-Rh.[1] The yellow crystals contain the five-coordinate complex $[Rh(acn)(tropp^{ph})_2]^+PF_6^-$ (**6**-Rh); the result of the X-ray structure analysis is shown in Figure 1. These yellow crystals easily decompose, with loss of acetonitrile, to give a red powder, as soon as they are separated from the mother liquor. The very high lability of **6**-Rh also prevents its detection by NMR spectroscopy as a stable species in solution (vide infra). Slightly yellow crystals of the iridium chloro complex **7**-Ir were grown from a concentrated solution in methylene chloride layered with *n*-hexane. The result of the X-ray structure analysis of **7**-Ir is shown in Figure 2. Selected bond lengths and angles of both complexes are given in the figure captions. Details concerning the data collection and refinement for **6**-Rh and **7**-Ir are compiled in Table 1.

Both compounds show the expected trigonal-bipyramidal structure with the two phosphorus atoms occupying the axial positions and the olefinic units, C=C_{trop}, occupying two of the equatorial positions. The bond lengths fall mostly within the typical range observed in comparable five-coordinate Rh^I and Ir^I complexes[22] and compare well with those in the hydride complex **4**.[20] The M–C and M–P distances are similar for both **6**-Rh and **7**-Ir. The acetonitrile ligand in **6**-Rh deviates by about 5.8° from linearity, pointing towards P1a, and the Rh–N bond is slightly longer than usual Rh–N single bonds.[22] For steric reasons, the C4a=C5a_{trop} unit

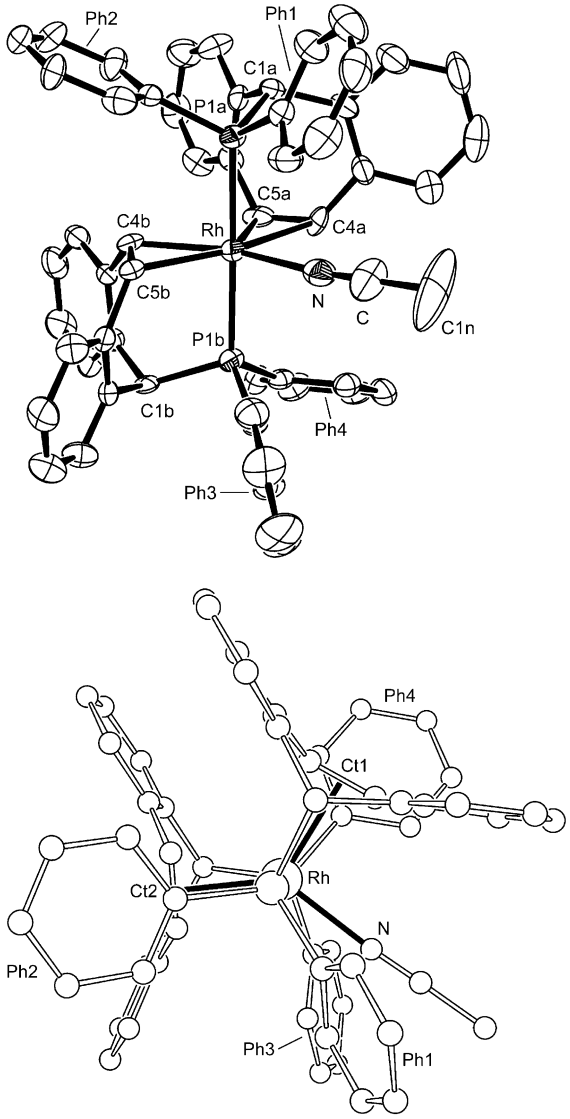

Figure 1. Top: Molecular structure and numbering scheme of the cation of $[Rh(acn)(tropp^{ph})_2]^+$ PF_6^- (**6**-Rh). Thermal ellipsoids are drawn at the 40% probability level. The hydrogen atoms and the counter ion (PF_6^-) are omitted for clarity. Bottom: View along the P1a-Rh-P1b vector. The connections between the Rh atom and the centroids Ct1 and Ct2 of the coordinated olefins C4a=C5a and C4b=C5b, respectively, and the Rh–N bond, are shown as solid lines. All atoms are drawn with arbitrary radii. Selected bond lengths [Å] and angles [°] for **6**-Rh: Rh–N 2.136(6), Rh–P1a 2.353(2), Rh–C4a 2.340(6), Rh–C5a 2.283(6), C4a–C5a 1.397(8), P1a–C1a 1.864(6), Rh–P1b 2.312(2), Rh–C4b 2.141(6), Rh–C5b 2.202(6), C4b–C5b 1.434(8), P1b–C1b 1.849(6), Rh–Ct1 2.203, Rh–Ct2 2.050, C4b–C5a 3.138; P1b-Rh-P1a 176.89(7), N-Rh-P1a 91.4(2), N-Rh-P1b 87.5(2), N-Rh-C4a 79.1(2), N-Rh-C5b 117.0(2), C4b-Rh-C5a 90.3(2); ω_1(N-Rh-Ct1) 96.4, ω_2(N-Rh-Ct2) 136.0, Ct1-Rh-Ct2 127.6.

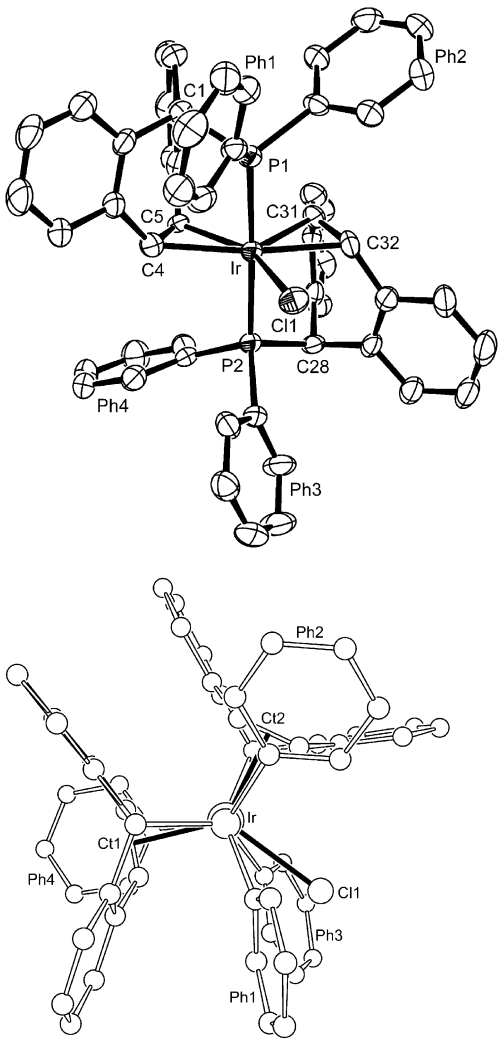

Figure 2. Top: Molecular structure and numbering scheme of $[IrCl(tropp^{ph})_2]$ (**7**-Ir). Thermal ellipsoids are drawn at the 40% probability level. The hydrogen atoms are omitted for clarity. Bottom: View along the P1-Ir-P2 vector. The connections between the Ir atom and the centroids Ct1 and Ct2 of the coordinated olefins C4=C5 and C31=C32, respectively, and the Ir-Cl bond, are shown as solid lines. All atoms are drawn with arbitrary radii. Selected bond lengths [Å] and angles [°] for **7**-Ir: Ir–Cl1 2.497(2), Ir–P1 2.321(2), Ir1–C4 2.198(6), Ir1–C5 2.134(6), C5–C4 1.454(9), Ir–P2 2.337(2), Ir–C31 2.190(6), Ir–C32 2.217(6), C31–C32 1.425(9); P1-Ir-P2 177.99(5), P1-Ir-Cl1 87.60(6), P2-Ir-Cl1 92.63(6), C4-Ir-Cl1 110.6(2), C32-Ir-Cl1 81.7(2), C5-Ir-C31 90.9(2), Ir–Ct1 2.041, Ir–Ct2 2.085; ω_1(Cl-Ir-Ct2) 100.4, ω_2(Cl-Ir-Ct1) 129.9, Ct1-Ir-Ct2 129.6.

forms a smaller angle with the Rh–N bond (ω_1(N–Rh–Ct1) = 96.4°, Ct1 = centroid of the C4a=C5a bond) and has a longer distance to the rhodium center (Rh–Ct1 = 2.203 Å), when compared to the other coordinated olefin bond C4b=C5b$_{trop}$ (Rh–Ct2 = 2.050 Å, Ct2 = centroid of the C4b=C5b bond). Correspondingly, the C4a=C5a distance (1.397(8) Å) is shorter than that of C4b=C5b (1.434(8) Å). In **7**-Ir, both C=C$_{trop}$ units are close to the iridium center (Ir–Ct1 = 2.041 Å, Ir–Ct2 = 2.085 Å) and the C=C bonds are elongated to >1.42 Å by metal-to-ligand backbonding. A view along the P-M-P axis reveals a rather strong deviation from an ideal trigonal arrangement (i.e., L-M-L angles of 120°) of the ligands in the equatorial plane towards a so called "Y/T"-shaped structure.[23,24] The nitrogen atom in **6**-Rh deviates by 14.8°, and the chloride atom in **7**-Ir by 19.8°, from the bisection of the Ct1-M-Ct2 angle (M = Rh, Ir; Ct1/2 = centroids of the C=C$_{trop}$ bonds). In the 18-electron complexes **6**-Rh and **7**-Ir this distortion certainly has exclusively steric reasons[25] and is only detected in the solid state. In solution, only two sets of signals are observed for the pairwise equivalent olefinic protons (see black and white circles in Scheme 2 below), even at low temperatures.

Table 1. Crystallographic and refinement details of **6**-Rh and **7**-Ir.

compound	**6**-Rh	**7**-Ir
formula	$C_{56}H_{45}F_6NP_3Rh$	$C_{58.25}H_{42}ClP_2Ir$
crystal size [mm]	0.40×0.06×0.06	0.20×0.10×0.02
crystal system	monoclinic	monoclinic
space group	$P2_1/c$	P2/c
a [Å]	11.395(3)	23.86(1)
b [Å]	16.638(4)	9.800(5)
c [Å]	25.905(5)	19.72(1)
β [°]	96.59(2)	94.09(1)
V [Å^3]	4879(2)	4600(4)
Z	4	4
ρ_{calcd} [M gm^{-3}]	1.418	1.490
μ [mm^{-1}]	0.510	7.102
index range	$0 \le h \le 10$	$-23 \le h \le 23$
	$0 \le k \le 16$	$0 \le k \le 9$
	$-24 \le l \le 24$	$0 \le l \le 19$
$2\theta_{max}$ [°]	40.08	49.94
T [K]	293	293
reflections	4572	4561
parameters	609	573
GOOF	0.763	1.056
final $R1$	0.0400	0.0396
final w$R2$ (all data)	0.0681	0.1083
max/min residual el. density [eÅ^{-3}]	0.587/−0.502	2.293/−0.764

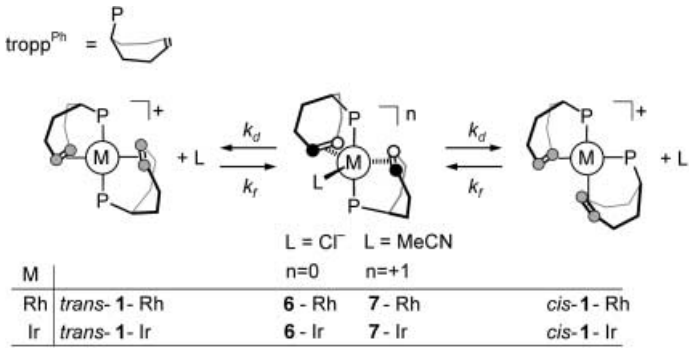

Scheme 2. Formation of five-coordinate tropp complexes **6**-M and **7**-M from *trans*-**1**-M or *cis*-**1**-M (M = Rh, Ir). Gray circles indicate magnetically equivalent olefin protons in *trans*/*cis*-**1**-M and black or white circles indicate the non-equivalent protons in **6**-M and **7**-M.

NMR studies: In a non-coordinating solvent like methylene chloride (CH_2Cl_2), the cationic four-coordinate complexes $[M(tropp^{Ph})_2]^+$ (M = Rh: **1**-Rh and M = Ir: **1**-Ir) with weakly coordinating counteranions like PF_6^-, BF_4^-, or $CF_3SO_3^-$, exist as mixtures of *trans* and *cis* isomers that do not interconvert on the NMR timescale.[26] In a coordinating solvent like acetonitrile, or in the presence of a coordinating anion like Cl^-, the four-coordinate complexes **1**-Rh and **1**-Ir give the five-coordinate complexes $[M(acn)(tropp^{Ph})_2]^+$ (M = Rh: **6**-Rh; M = Ir: **6**-Ir) and $[MCl(tropp^{Ph})_2]$ (M = Rh: **7**-Rh; M = Ir: **7**-Ir) (Scheme 2). With the exception of $[Rh(acn)(tropp^{Ph})_2]^+$ (**6**-Rh), the formation can be easily followed by ^{1}H, ^{13}C, ^{31}P, and ^{103}Rh NMR spectroscopy and selected NMR data are listed in Table 2. The formation of **6**-Rh is only indicated indirectly, as the $^1J(^{103}Rh,^{31}P)$ coupling constant, and the chemical shift of the olefinic CH=CH$_{trop}$ protons of the *trans* isomer depend on the acetonitrile concentration and the temperature (that is, at $T = 223$ K, $\delta(^1H)$ is shifted from 5.66 ppm in pure CD_2Cl_2 to 4.36 ppm in a 1:1 mixture of CD_2Cl_2/CD_3CN). Note that the *cis*-$[Rh(tropp^{Ph})_2]^+$ complex is not affected either by a variation of the temperature or by the concentration of acetonitrile. Similiar observations were made when the iridium complexes *trans*/*cis*-$[Ir(tropp^{Ph})_2]^+$ (*trans*/*cis*-**1**-Ir) were dissolved in THF at $T = 298$ K. Only the ^{31}P resonance of the *trans* isomer is broadened, while that of the *cis* isomer remains sharp.[27]

In solution, the olefinic protons and ^{13}C nuclei in the four-coordinate $[M(tropp^{ph})_2]^+$ complexes, **1**-Rh and **1**-Ir, are isochronous (gray circles in Scheme 2), indicating square-planar structures on the on average over time. The ^{1}H and ^{13}C resonances of the coordinated olefins in the *cis* isomers of **1**-Rh and **1**-Ir appear at higher frequencies, relative to the *trans* isomers; this may be taken as an indication of weaker M→L backbonding, probably as a result of the higher *trans* influence of a P donor relative to an olefin. Steric congestion may also play a role.[28,29]

In comparison to the four-coordinate species, the ^{31}P and, especially, the ^{1}H and ^{13}C NMR resonances, of the five-coordinate complexes are significantly shifted to lower frequencies, indicating enhanced M→L backbonding. In accordance with the structures of the five-coordinate complexes (vide supra), the ^{1}H and ^{13}C NMR resonances of the olefinic C=C$_{trop}$ unit in **6**-Ir, **7**-Rh, and **7**-Ir are inequivalent (see black and white circles in Scheme 2). The protons appear as two multiplets, corresponding to the AA′ and BB′ parts of an AA′BB′XX′ spin system (XX′ = phosphorus nuclei). Accordingly, two multiplets for the olefinic ^{13}C nuclei are observed. A comparison between the iridium complexes $[Ir(L)(tropp^{Ph})_2]^n$ (**6**-Ir: L = acn, $n = +1$; **7**-Ir: L = Cl^-, $n = 0$; **4**-Ir: L = H^-, $n = 0$;[20] **8**[20]: L = CO, $n = +1$:) is instructive: The

Table 2. Selected ^{103}Rh, ^{31}P, ^{13}C, and ^{1}H NMR data. For the rhodium complexes *trans*/*cis*-**1**-Rh and **7**-Rh, the $^1J(^{103}Rh,^{31}P)$ couplings [Hz] are given in parentheses.

	solvent	T [K]	δ^{31}P	δ^{13}C(olefin)	δ^1H(olefin)	δ^{103}Rh
			four-coordinate 16-electron complexes			
trans-**1**-Rh	CD_2Cl_2	248	85.8 (131)	85.7	5.66	210
cis-**1**-Rh	CD_2Cl_2	248	83.7 (178)	106.1	6.50	−253
trans-**1**-Ir	CD_2Cl_2	298	72.8	71.0	5.41	
cis-**1**-Ir	CD_2Cl_2	298	68.8	87.0	5.86	
			five-coordinate 18-electron complexes			
6-Ir[a]	CD_3CN	233	53.4	48.9, 46.5	4.17, 3.89	
7-Rh	CD_2Cl_2	213	81.3 (117)	67.1, 64.9	4.56, 3.90	381
7-Ir	$CDCl_3$	298	48.1	48.7, 43.9	4.10, 3.45	
4[b]	CD_2Cl_2	298	73.3	36.8, 34.7	3.06, 2.73	
8[b]	$CDCl_3$	298	53.9	61.3, 61.0	4.54, 3.62	

[a] The synthesis and isolation of **6**-Ir was reported in ref. [20], where the exchange-broadened NMR data at 298 K were given. [b] **4** = $[IrH(tropp^{ph})_2]$.[20] **8** = $[Ir(CO)(tropp^{ph})_2]^+PF_6^-$.[20]

strongly σ-donating hydride ligand in $[IrH(tropp^{ph})_2]$ (**4**) shifts the ^1H and ^{13}C NMR resonances to the lowest frequency values in this series of iridium complexes, while the strongly π-accepting CO does the opposite. The values for the complexes **6**-Ir and **7**-Ir fall in between the two extremes marked by **4** and **8**. The data for both **6**-Ir and **7**-Ir are very similar and thus imply similar electronic properties.

Dynamic NMR studies: We investigated the formation and dissociation of the five-coordinate complexes $[RhCl(tropp^{Ph})_2]$ (**7**-Rh), $[Ir(acn)(tropp^{Ph})_2]^+$ (**6**-Ir), and $[IrCl(tropp^{Ph})_2]$ (**7**-Ir) in more detail, by performing line-shape analyses (LSA)[30] or spin-inversion experiments according to the Forsén–Hoffman magnetization-transfer technique (FHMT).[31] We begin our discussion with the dissociation of the 18-electron $[RhCl(tropp^{Ph})_2]$ complex (**7**-Rh) into the four-coordinate 16-electron complexes *trans*-**1**-Rh [Eq. (2)] and *cis*-**1**-Rh [Eq. (3)].At ambient temperature in CD_2Cl_2, only one broadened doublet is observed in the ^{31}P NMR spectrum for **7**-Rh. On cooling to about 253 K this broadens further, then starts to sharpen. At the same time, two additional doublets appear with low intensity at higher frequencies; these are characteristic of *cis*-**1**-Rh and *trans*-**1**-Rh (see Table 2). In order to enhance the concentration of the cationic species *cis*-**1**-Rh and *trans*-**1**-Rh, to allow for a more accurate determination of their concentration by integration of the NMR signals, the equilibria in Equations (2) and (3) were studied in CD_2Cl_2 containing different amounts of $(nBu_4N)PF_6$ as electrolyte (0.031 M, 0.067 M, 0.103 M). These experiments also give qualitative information about the influence of the polarity of the reaction medium. All species, **7**-Rh, *trans*-**1**-Rh, and *cis*-**1**-Rh are observed directly by NMR spectroscopy and therefore the data for both equilibria could be obtained.[32]

$$[RhCl(tropp^{Ph})_2] \rightleftharpoons \underset{\textit{trans}\text{-}\mathbf{1}\text{-Rh}}{\textit{trans}\text{-}[Rh(tropp^{Ph})_2]^+} + Cl^- \qquad (2)$$
7-Rh

$$[RhCl(tropp^{Ph})_2] \rightleftharpoons \underset{\textit{cis}\text{-}\mathbf{1}\text{-Rh}}{\textit{cis}\text{-}[Rh(tropp^{Ph})_2]^+} + Cl^- \qquad (3)$$
7-Rh

In Figure 3, selected ^{31}P spectra at four different temperatures and two different salt concentrations (0.031 M and 0.067 M $(nBu_4N)PF_6$) are shown. Beside each experimental spectrum, the simulated spectrum is displayed, demonstrating the high quality of the simulation. The effect of the temperature and electrolyte concentration is immediately evident: raising the temperature and/or salt concentration leads to increasing amounts of the ionic products. Furthermore, line broadening, especially for *trans*-**1**-Rh and **7**-Rh, is observed with increasing temperatures. The equilibrium constant, K_d, and thermodynamic parameters for the dissociation reactions in equilibria in Equations (2) and (3) are listed in Table 3.

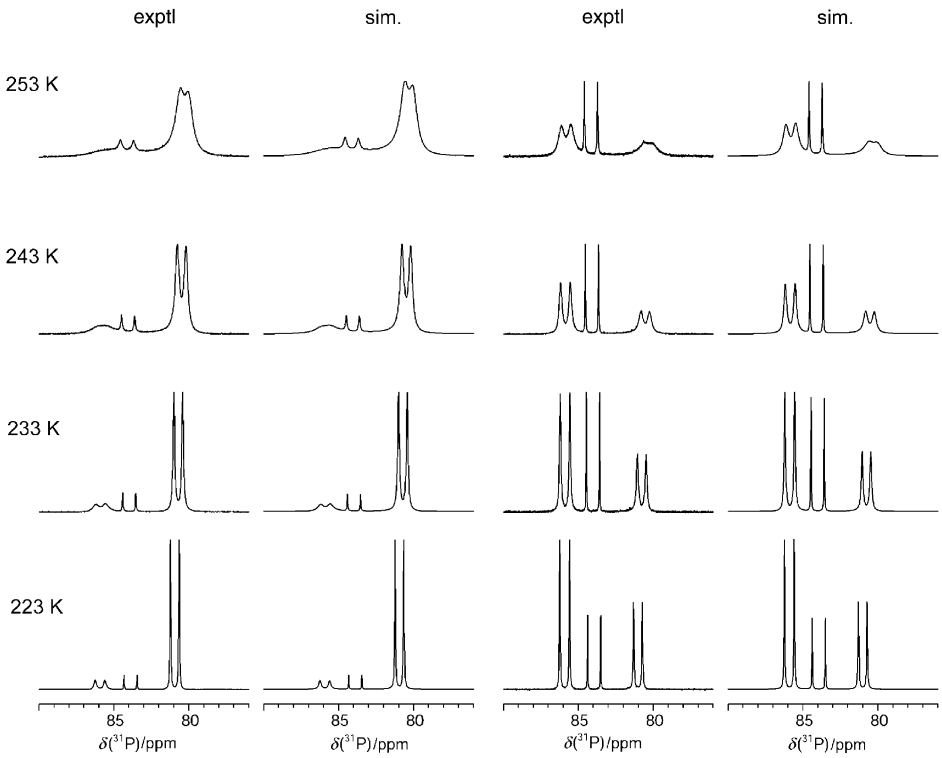

Figure 3. The first and third column shows the experimental 202 MHz $^{31}P\{^1H\}$ NMR spectra for $[RhCl(tropp^{ph})_2]$ in CD_2Cl_2 at four different temperatures. $[Rh]_{tot}$ was 0.10 M to which $(nBu_4N)PF_6$ had been added in concentrations of 0.031 M (left side) and 0.067 M (right side), respectively. The second and fourth columns represent the simulations of the experimental spectra to their left using the MEXICO program package,[30] which were used to obtain the thermodynamic and kinetic parameters for the exchange reactions shown in Equations (2) and (3).

The dissociation reactions in Equations (2) and (3) are endogonic. Although activation enthalpies and entropies deter-

Table 3. Thermodynamic parameters for the equilibria in Equations (2) and (3) at $T = 298$ K.

$(nBu_4N)PF_6$ [M]	K_d^{298} [M]	ΔG_d^o [kJ mol^{-1}]	$\Delta H°$ [kJ mol^{-1}]	$\Delta S°$ [J mol^{-1} K^{-1}]
	$[RhCl(tropp^{Ph})_2] \rightarrow \textit{trans}\text{-}[Rh(tropp^{Ph})_2]^+ + Cl^-$			
0.031	1.1×10^{-2}	11.2	6.1	−17.0
0.067	2.2×10^{-2}	9.5	5.9	−12.0
0.103	1.4×10^{-1}	4.8	2.6	−7.6
	$[RhCl(tropp^{Ph})_2] \rightarrow \textit{cis}\text{-}[Rh(tropp^{Ph})_2]^+ + Cl^-$			
0.031	3.3×10^{-3}	14.1	6.8	−24.4
0.067	7.5×10^{-3}	12.1	6.3	−19.4
0.103	4.4×10^{-2}	7.8	2.3	−18.4

mined by NMR methods must be regarded with great care,[33] our data indicate that the enthalpies ($\Delta H°$) are mainly influenced by the polarity of the reaction medium. As expected for a process in which a neutral compound dissociates into charged species, $\Delta H°$ becomes smaller (less positive) with increasing polarity of the medium and the dissociation entropies are negative, indicating higher order solvation spheres for the ionic products.

Because the first-order dissociation rate constants (k_d), that is, the forward reactions in Equations (2) and (3), are better suited for comparison, these were calculated and used in classical Eyring plots ($R\ln(kh/k_bT)$ vs. $1/T$) to obtain the activation energy $\Delta G^{\#}(T)$ [kJ mol^{-1}] (see Experimental Section for details). As an example, the graph for the dissociation of the five-coordinate chloro complex **7**-Rh into *trans*-**1**-Rh is shown in Figure 4. Note that, in agreement with the

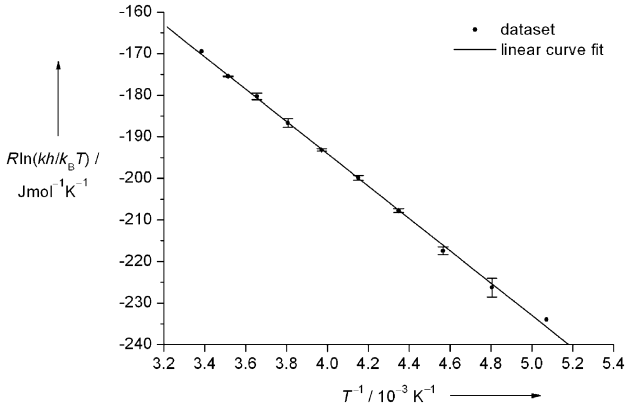

Figure 4. Eyring plot, $R\ln(kh/k_BT)$ versus the inverse temperature T^{-1}, giving $\Delta G^{\#} = 50.3$ kJ mol^{-1} for the dissociation of [RhCl(tropp^{ph})$_2$] to *trans*-[Rh(tropp^{ph})$_2$]$^+$ [Eq. (2)].

assumption that this process obeys a first-order rate law and, hence, k_d is independent of the concentration of [**7**-Rh], the data for the three different electrolyte concentrations fall onto one line.

The dissociation of **7**-Rh to the *cis*-configured cation is more strongly endogonic than that to the *trans* isomer. An evaluation of the data shows that **7**-Rh dissociates about 40 times slower to the *cis* complex than to the *trans* complex (see entries 1 and 2 in Table 4). Hence, the finding that the NMR signals for *cis*-**1**-Rh remain significantly sharper at all temperatures and electrolyte concentrations is due to the fact that the equilibrium reactions in Equation (3) are one order of magnitude slower than those in Equation (2).

The higher activation barrier for *cis*-**1**-Rh [$\Delta(\Delta G^{\#}_{cis-trans}) = 7.8$ kJ mol^{-1}] is probably due to the fact that, apart from Rh–Cl bond rupture, a considerable rearrangement of the ligand sphere, that is, a type of Turnstile rotation, must also occur. On the other hand, the formation of *trans*-**1**-Rh is pre-organized in the structure of **7**-Rh.

Within experimental error, the same rate constants k_d and activation energies $\Delta G^{\#}$ as discussed before were obtained from the resonances of the benzylic protons at the 5-position

Table 4. Dissociation rate constants k_d and activation energies $\Delta G^{\#}(T)$ for equilibria (2)–(6).

	Eq.	T [K]	k_d [s^{-1}]	$\Delta G^{\#}$ [kJ mol^{-1}][a]	Method
1	(2)	295	≈8640	50.3	LSA[b]
2	(3)	295	≈238	58.1	LSA[b]
3	(4)	298	5[c]	69.8	SI (FHMT)[c]
4	(5)	298	8	67.7	LSA[d]
5	(6)	298	3700	53.1	LSA[d]

[a] The activation energies were obtained from Eyring plots [$R\ln(k_dh/k_BT)$ vs. $1/T$] (see Figure 4 for an example). [b] The ^{31}P NMR resonances (Figure 3) were used in line shape analyses (LSA) using the MEXICO program package for the determination of k_d at different temperatures. [c] Spin inversion (SI) ^{31}P NMR experiments [Forsén–Hoffman type magnetization transfer (FHMT)] were performed, and the resulting points fitted with the CIFIT program package to determine the rate constant for the ligand exchange reaction in Equation (4) (Figure 5). [d] The olefinic CH=CH$_{trop}$ ^{1}H NMR resonances (Figure 6) were used in line shape analyses (LSA) using the MEXICO program package for the determination of k_d at different temperatures.

of the dibenzo[*a*,*d*]cycloheptene instead of the ^{31}P resonances in an LSA. As the resonances of the olefinic protons in the CH=CH$_{trop}$ units are very broad and overlap, they cannot be used in a simulation. However, a qualitative inspection of the line shape reveals that a process with a rate constant approximately ten times *larger* (i.e., the $\Delta G^{\#}$ for this process is about 6 kJ mol^{-1} lower in energy) leads to an equilibration of these signals. This finding is incompatible with the assumption that the exchange between the olefinic protons occurs solely by a simple unimolecular dissociation process in which the dissociated solvated chloride ion adds rapidly either from the front or back side of the four-coordinate product complexes *trans*/*cis*-**1**-Rh. A second process (process A), including complete dissociation of one C=C$_{trop}$ unit in **7**-Rh and flipping of one tropp ligand from one side to the other, may be responsible for this phenomenon. Alternatively, a close ion pair {[Rh(tropp^{Ph})$_2$]$^+$Cl$^-$} may be formed in a pre-equilibrium (process B) [RhCl(tropp^{Ph})$_2$]⇄{[Rh(tropp^{Ph})$_2$]$^+$Cl$^-$} before the dissociation of the chloro ligand is completely accomplished.[34] Since the "chloride" in such an ion pair should be very mobile, positional exchange of the olefin protons with a smaller barrier than that for dissociation may occur. Our data do not allow us to distinguish between these two possibilities with certainty. However, in view of the considerable steric crowding (see Figures 1 and 2) and the finding that the dissociation giving *cis*-**1**-Rh requires a comparable reorganization of the ligand sphere that actually has a higher activation barrier, leads us to favor the close-ion-pair formation, that is, process B.

A solution of the five-coordinate iridium complex [IrCl(tropp^{Ph})$_2$] (**7**-Ir) in CD_2Cl_2 shows sharp ^{31}P and ^{1}H NMR signals at all temperatures between $T = 223$ K and 318 K and no dynamic phenomenon is observed. Hence, the dissociation into the four-coordinate ions *trans*- and *cis*-[Ir(tropp^{Ph})$_2$]$^+$ (*trans*/*cis*-**1**-Ir) and Cl$^-$ cannot be observed directly by NMR spectroscopy. Therefore the ligand exchange reaction [Eq. (4)] between the chloro complex **7**-Ir and ace-

tonitrile complex **6**-Ir was investigated in CH_2Cl_2 containing various amounts of acetonitrile.

$$[IrCl(tropp^{Ph})_2] + acn \rightleftharpoons [Ir(acn)(tropp^{Ph})_2]^+ + Cl^- \quad (4)$$
7-Ir **6**-Ir

It is assumed that this reaction proceeds stepwise through the dissociation of the chloro complex **7**-Ir into the cationic complexes *trans*/*cis*-$[Ir(tropp^{Ph})_2]^+$ [Eq. (5)], which subsequently react with acetonitrile to give **6**-Ir. The equilibrium constant $K_r^{(4)}$ of the ligand exchange reaction [Eq. (4)] was measured at various temperatures and a van't-Hoff plot ($-R\ln K_r^{(4)}$ vs. $1/T$) gave $\Delta H° = -26.1\ kJ\,mol^{-1}$ and $\Delta S° = -116.8\ J\,mol^{-1}\,K^{-1}$. Although the data must again be interpreted with care,[33] they indicate that the cationic acetonitrile complex **6**-Ir may be enthalpically favored, but a negative entropy makes the substitution in Equation (4) endogonic ($\Delta G° = 8.7\ kJ\,mol^{-1}$ at $T = 298\ K$) and stabilizes the chloro-complex **7**-Ir.

$$[IrCl(tropp^{Ph})_2] \rightleftharpoons trans/cis\text{-}[Ir(tropp^{Ph})_2]^+ + Cl^- \quad (5)$$
7-Ir *trans*/*cis*-**1**-Ir

A UV-visible titration of a solution of the four-coordinate complexes *trans*/*cis*-$[Ir(tropp^{Ph})_2]^+$ (*trans*/*cis*-**1**-Ir) in CH_2Cl_2 with acetonitrile furnishes the formation equilibrium constant, $K_f^{(6)} = 626\ M^{-1}$, for the reaction given in Equation (6). The equilibrium constant, $K_d^{(5)}$, and the free reaction energy ΔG_d^o for the dissociation reaction [Eq. (5)] of the iridium chloro complex can then be calculated according to $K_d^{(5)} = K_r^{(4)}/K_f^{(6)} = 0.0337/626 = 5.8 \times 10^{-5}\ M$ at $T = 298\ K$ ($\Delta G_d^o = 24\ kJ\,mol^{-1}$). These data show that the five-coordinate iridium complex **7**-Ir is considerably more stable than the analogous rhodium complex **7**-Rh (c.f. $\Delta G_d^o \approx 4.8$–$14.1\ kJ\,mol^{-1}$ in Table 3).

$$trans/cis\text{-}[Ir(tropp^{Ph})_2]^+ + acn \rightleftharpoons [Ir(acn)(tropp^{Ph})_2]^+ \quad (6)$$
trans/*cis*-**1**-Ir **6**-Ir

The exchange rate for the ligand exchange reaction in Equation (4) is comparable with the spin-lattice relaxation time T_1. As a consequence, the line broadening is too small to allow a LSA to give sufficiently exact data. Therefore, a spin-inversion experiment was performed in which the ^{31}P NMR signal of the chloro complex **7**-Ir was inverted by a selective 180° pulse. Because **7**-Ir and **6**-Ir are exchange-coupled, the inversion affects the ^{31}P NMR signal intensity of **6**-Ir. The time to recover to the equilibrium state is dependent on T_1 and the exchange rate k. This process was followed by measuring the magnetization of the sample after spin inversion at various time intervals (Forsén–Hoffman magnetization transfer technique (FHMT)[31]). Two typical curves at temperatures $T = 293\ K$ and $T = 313\ K$ are shown in Figure 5. The rate constants (k_{obs}), as a function of temperature, for the forward reaction $[IrCl(tropp^{Ph})_2]$ (**7**-Ir) + acn → $[Ir(acn)(tropp^{Ph})_2]^+$ (**6**-Ir) + Cl^- were obtained by curve fitting with the CIFIT program package[32] and used to determine (Eyring plot) the free activation energy $\Delta G^{\#} =$

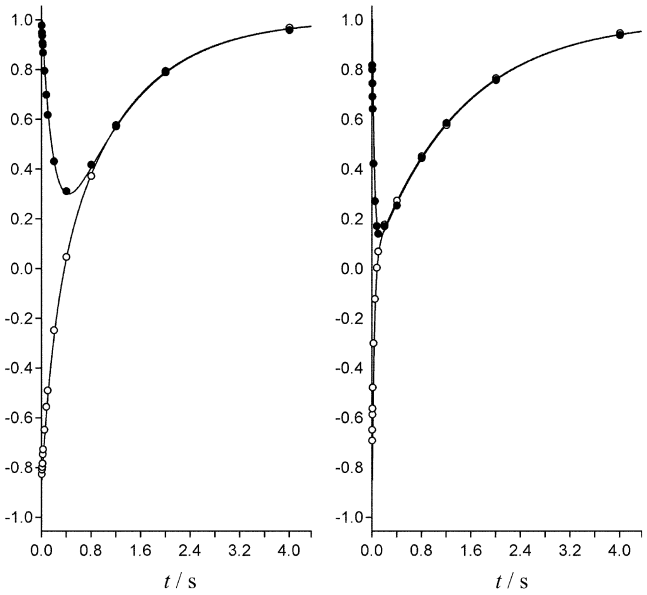

Figure 5. Monitored experimental intensities, open and filled circles for the resonances of $[IrCl(tropp^{ph})_2]$ (inverted) and $[Ir(acn)(tropp^{ph})_2]^+$, respectively, from the 202 MHz $^{31}P\{^1H\}$ magnetization transfer experiments for the ligand exchange process described in Equation (4) at 293 K (left) and 313 K (right). The biexponential curves drawn represent the fits as obtained from the CIFIT program package,[32] giving exchange rates of $2.6\ s^{-1}$ and $15.2\ s^{-1}$ at 293 K and 313 K, respectively.

$69.8\ kJ\,mol^{-1}$ (Table 4). It is assumed that the dissociation of the chloro complex **7**-Ir is the rate-determining step in Equation (4) and that the observed rate constant (k_{obs}) equals the rate constant k_d' of the dissociation to the four-coordinate complexes *trans*/*cis*-$[Ir(tropp^{Ph})_2]^+$ (*trans*/*cis*-**1**-Ir). The dissociation into both isomers cannot be separately observed, but we assume that $k_d' = k_d(trans) + k_d(cis) \approx k_d(trans)$, as $k_d(cis) \ll k_d(trans)$ (see the discussion of the analogous rhodium complexes and of the $[Ir(thf)(tropp^{Ph})_2]$ complex above and in the footnotes).[27] That these square-planar complexes are very likely the intermediates in the ligand displacement reactions, indeed, is indirectly indicated by the exchange of the diastereotopic olefinic proton resonances in **7**-Ir and **6**-Ir (see the white and black circles in Scheme 2) that is observed in the ^1H NMR spectra. This observation requires either an intermediate with a mirror plane to participate in the equilibrium in Equation (4) or a highly fluxional behavior of the five-coordinate species $[IrL(tropp^{Ph})_2]$. While the latter possibility could not be ruled out for the rhodium complexes discussed above, we exclude this possibility for the iridium complexes, because, as mentioned above, $[IrCl(tropp^{Ph})_2]$ (as well as $[IrH(tropp^{Ph})_2]$[20]) shows sharp and well-resolved NMR signals in the absence of a coordinating solvent, indicating the integrity and non-fluxional behavior of these compounds.

In Figure 6, the signals for the $CH{=}CH_{trop}$ protons in the ^1H NMR spectra for the chloro (**7**-Ir) and acetonitrile (**6**-Ir) complexes are displayed at various temperatures. On the right hand side the simulated spectra are shown, again demonstrating the excellent fit with the experimental data. While separated multiplets are observed for **7**-Ir up to 318 K, those for the acetonitrile complex are observed as an

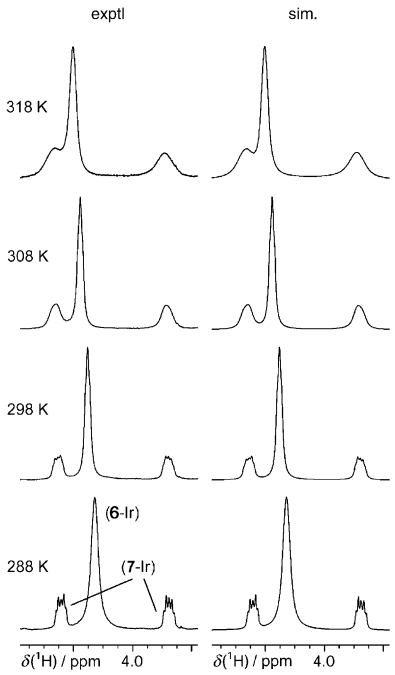

Figure 6. Experimental and simulated (using the MEXICO program package[30]) 500 MHz variable temperature ^{1}H NMR spectra of a mixture of [IrCl(tropp^{ph})$_2$] and [Ir(acn)(tropp^{ph})$_2$]$^+$. Three dynamic process are distinguishable: i) slow exchange, on the NMR timescale, of the diastereotopic olefinic protons in [IrCl(tropp^{ph})$_2$] (**7**-Ir); ii) fast exchange of the same type of protons in [Ir(acn)(tropp^{ph})$_2$]$^+$ (**6**-Ir); and iii) exchange between these two complexes according to Equation (4).

averaged signal (broadened resonance at $\delta = 4.4$ ppm) due to more rapid exchange. Quantitative kinetic data for the reaction **7**-Ir $\rightarrow$ *trans*/*cis*-**1**-Ir + Cl$^-$ [forward reaction in Eq. (5)] and **6**-Ir $\rightarrow$ *trans*/*cis*-**1**-Ir + acn [backward reaction in Eq. (6)] were obtained by line shape analyses and Eyring plots, and these are listed in Table 4. Clearly, the activation energies for the processes in Equations (4) ($\Delta G^{\#} = 69.8$ kJ mol^{-1}) and (5) ($\Delta G^{\#} = 67.7$ kJ mol^{-1}) are very similar. The dissociation barrier for the acetonitrile complex in Equation (6) is much lower ($\Delta G^{\#} = 53.1$ kJ mol^{-1}). With the dissociation rate constant (3.7×10^3 s^{-1}, see Table 4, entry 5) and the equilibrium constant, $K_f^{(6)} = 626$ M^{-1}, the rate constant for the formation of the iridium acetonitrile complex **6**-Ir is calculated according to $k_f = K_f^{(6)} \times k_d = 2.3 \times 10^6$ M^{-1} s^{-1}. This rate constant is six orders of magnitude larger than the rate constant for the dissociation of the chloro complex, which is the rate-determining step in the ligand exchange reaction [Eq. (4)], as we assumed.

Electrochemical Investigations

With these thermodynamic and kinetic data at hand, we looked in more detail at the electrochemistry of the [M(tropp^{Ph})$_2$]$^+$ complexes (M = Rh, Ir). Orsini and Geiger showed recently, on a related system, that electrochemical techniques are a powerful tool for the determination of fundamental thermodynamic and kinetic data in ligand displacement reactions, provided that one of the species participating in the equilibrium is electroactive.[35] Under our conditions, we find that donor solvents like THF or acetonitrile have no measurable effect on the electrochemical response in cyclic voltammograms (CVs) of [Rh(tropp^{Ph})$_2$]$^+$ (*trans*/*cis*-**1**-Rh). In all cases the already known[1] two quasi-reversible redox waves were observed. However, the CVs of the analogous iridium complexes [Ir(tropp^{Ph})$_2$]$^+$ (*trans*/*cis*-**1**-Ir) are solvent dependent.[2]

We used square-wave voltammetry to benefit from the high immunity of this method towards charging currents when fitting a large number of experimental voltammograms to simulated ones without the need to correct the background currents in the experimental data. One of us (M.R.) especially extended the available DIGISIM program suite[36] to allow the digital data simulation of SW voltammograms and the theoretical background is given in reference [37]. In Scheme 3, the possible pathways [Eqs. (6)–(11)] that interconnect the iridium–tropp complexes d^8 *trans*/*cis*-**1**-Ir, d^9 *trans*/*cis*-**2**-Ir, and d^{10} **3**-Ir with various formal metal oxidation states are presented. The predominant reactions [Eqs. (6), (7), (8), (9′) and (10)] are highlighted by black arrows. The thermodynamic and kinetic data as determined by the methods discussed above are also included. The rate and equilibrium constants for the reaction of *trans*/*cis*-**1**-Ir with acetonitrile [Eq. (6)] were estimated as described above in this work. The equilibrium constant K_i for the *trans*$\rightleftarrows$*cis* isomerization [Eq. (8)] of the paramagnetic d^9-[Ir(tropp^{Ph})$_2$] complexes stems from temperature-dependent recorded EPR spectra.[19] Importantly, the equilibrium in Equation (10) was included in the mechanism which was used for the simulation. The thermodynamic data for this process, that is, the equilibrium constants for the sympropportionation, $K_{symp} = e^{-(nF/RT)\Delta E} = 3.7 \times 10^4$, and disproportionation reactions, $K_{disp} = 1/K_{symp} = 2.7 \times 10^{-5}$, are easily deduced from the potential difference $\Delta E = E^{\circ 2} - E^{\circ 1} = -0.27$ V for the two redox processes given by Equations (7) ($E^{\circ 1} = -0.65$ V) and (9) ($E^{\circ 2} = -0.92$ V).

Figure 7 compares experimental (solid lines) square-wave (SW) voltammograms of *trans*/*cis*-[Ir(tropp^{Ph})$_2$]$^+$ (*trans*/*cis*-**1**-Ir) with simulated ones (open circles) computed on the basis of the set of reactions depicted in Scheme 3 by using the simulation algorithm described in reference [37]. The measurements were taken either in CH_2Cl_2 (A) or CH_2Cl_2 containing different amounts of acetonitrile [(B) 0.0375 M, (C) 0.17 M, (D) 0.73 M]. In the absence of acetonitrile, the voltammograms of *trans*/*cis*-[Ir(tropp^{Ph})$_2$]$^+$ (*trans*/*cis*-**1**-Ir) in CH_2Cl_2 solution exhibit two one-electron reduction steps (Figure 7A). The first one is almost diffusion controlled and the rate constant of the charge-transfer reaction amounts to about 0.2 cm s^{-1}. The second charge-transfer reaction is not diffusion controlled at high square frequencies and the height of the second square-wave peak decreases with increasingly high square-wave frequencies. The dependence of the peak height on the square-wave frequency is in agreement with the assumption that the first wave originates from the reduction of *trans*-[Ir(tropp^{Ph})$_2$]$^+$, the major component of the 16-electron complexes *trans*/*cis*-**1**-Ir [Eq. (7) in Scheme 3], while the second one results from the reduction of the 17-electron complex *cis*-[Ir(tropp^{Ph})$_2$]^0 (*cis*-**2**-Ir)

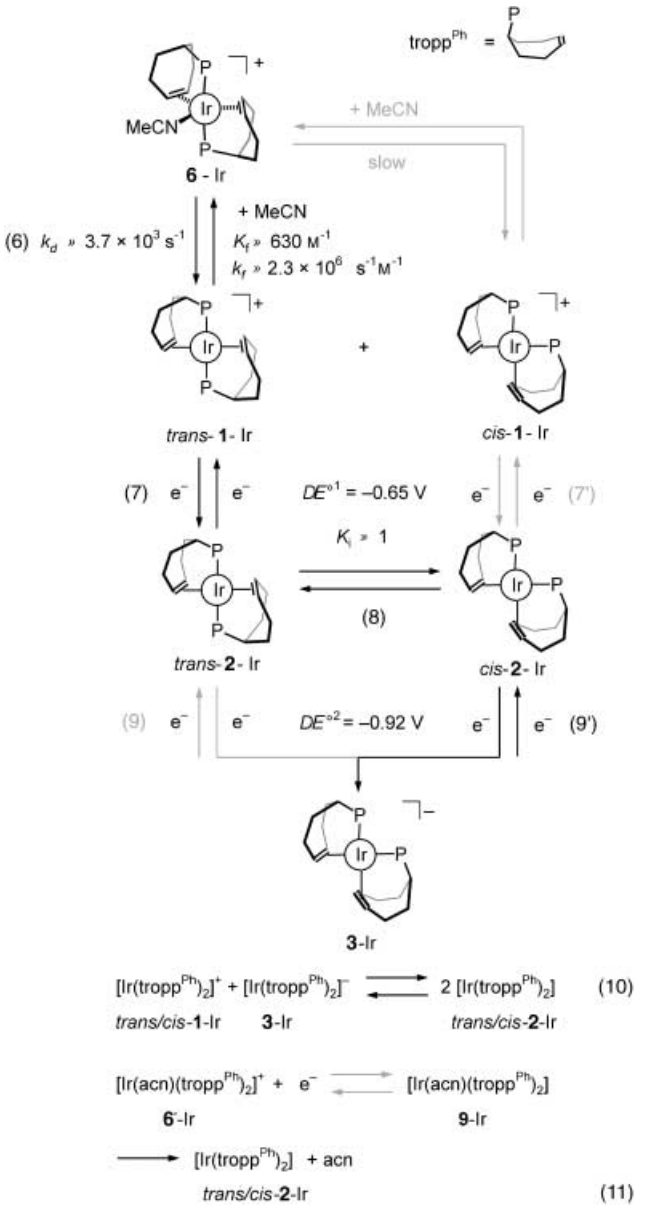

Scheme 3. Reaction diagram indicating the equilibria and redox reactions that connect the four- and five-coordinate iridium complexes in various formal oxidation states. The major reaction pathways are indicated by black arrows.

[Eq. (9′) in Scheme 3]. The finite speed of the *trans–cis* conversion [Eq. (8) in Scheme 3] at the stage of the 17-electron complexes, that is, from *trans*-$[Ir(tropp^{Ph})_2]^0$ (formed in the reduction step from *trans*-$[Ir(tropp^{Ph})_2]^+$) to *cis*-$[Ir(tropp^{Ph})_2]^0$, causes the second peak to become smaller with increasing square-wave frequency. This picture is completely reversed in the presence of acetonitrile. As can be seen in Figure 7B–D, the first peak becomes increasingly small with increasing acetonitrile concentration and/or increasing square-wave frequency. This behavior can be explained by the formation of the adduct $[Ir(acn)(tropp^{Ph})_2]^+$ (**6**-Ir), which is not reducible in the potential range shown in Figure 7 and is only formed by the cationic $[Ir(tropp^{Ph})_2]^+$ complexes. The reduced, neutral $[Ir(tropp^{Ph})_2]^0$ species do not form stable adducts (vide infra). At high acetonitrile concentrations (Figure 7D) the current of the first wave is mostly governed by the rate of the dissociation reaction [Eq. (6)] of the acetonitrile adduct and therefore almost independent of the square-wave frequency.

It is noteworthy that the shoulder that appears in the square-wave voltammograms at high acetonitrile concentrations (see Figure 7D) and low square-wave frequencies at about −0.85 V is not related to the formation of an additional species. However, the observation of such a shoulder is in perfect agreement with the simulated curves if a homogeneous electron transfer [Eq. (10)] is assumed to proceed between the fully reduced 18-electron anionic species **3**-Ir diffusing away from the electrode and the cationic 16-electron species *trans/cis*-**1**-Ir diffusing to the electrode surface. The computed equilibrium and rate constants for the reactions in Equations (6), (8), and (10) are compiled in Table 5.

Table 5. Simulated thermodynamic and kinetic data from square-wave voltammograms of *trans/cis*-$[Ir(tropp^{Ph})_2]^+$ (*trans/cis*-**1**-Ir) at $T = 298$ K. "f" indicates the forward and "b" the backward reaction of the given equilibria in Equations (6), (8), and (10) in Scheme 3.

Equation	K	k_f	k_b
(6)	620–520 [M^{-1}]	$(3.6–2.5)\times10^6$ [M^{-1}s^{-1}]	$(5.8–4.8)\times10^3$ [s^{-1}]
(8)	≈1	$\approx1\times10^4$ [s^{-1}]	$\approx1\times10^4$ [s^{-1}]
(10)	$\approx3.7\times10^4$	$\approx5\times10^8$ [M^{-1}s^{-1}]	$\approx1.4\times10^4$ [M^{-1}s^{-1}]

For the reaction in Equation (6), K corresponds to the equilibrium constant for the formation, k_f to the rate constant for the formation, and $k_b = k_d$ to the rate constant for dissociation of the five-coordinate acetonitrile complex $[Ir(acn)(tropp^{Ph})_2]^+$ (**6**-Ir). These data agree very satisfactorily with the values independently determined by the UV-visible and NMR experiments (see Scheme 3). With the equilibrium constant $K_i \approx 1$ (EPR measurements)[19] for the *trans*/*cis* isomerization [Eq. (8)] of the 17-electron complexes $[Ir(tropp^{Ph})_2]^0$ (**2**-Ir), the simulation gives the rate constant $k_f = k_b = k_i \approx 1\times10^4$ s^{-1}. This rather fast process indicates that the energy difference between the distorted square-planar and a more tetrahedral transition-state structure is small for four-coordinate rhodium(o) and iridium(o) complexes.

Due to the good agreement between the equilibrium and rate constants determined by different physical methods, the data for the symproportionation/disproportionation reaction [Eq. (10)] can also be regarded with some confidence. A rate constant $k_f = k_{homo} = 5\times10^8$ M^{-1}s^{-1} is obtained. With the equilibrium constant $K_{disp} = 2.7\times10^{-5}$, the rate constant $k_b = k_{disp} = (k_{homo}\times K_{disp}) = 1.4\times10^4$ M^{-1}s^{-1} for the reverse disproportionation reaction is calculated. Although this reaction is four orders of magnitude slower than k_{homo}, it is sufficiently fast to support the idea that the paramagnetic 17-electron complexes $[Ir(tropp^{Ph})_2]^0$ are not directly involved in the reactions with hydrogen or protons, as is shown in Scheme 1. Instead the closed-shell species participating in the redox equilibrium in Equation (10) are the truly reactive species. A similar conclusion, that is, that d^9-$[ML_4]^0$ complexes (M = Rh, L = $Ph_2P(CH_2)_2PPh_2$ = dppe) might be quite unreactive, has indeed been drawn by Eisenberg et al. some time ago.[38]

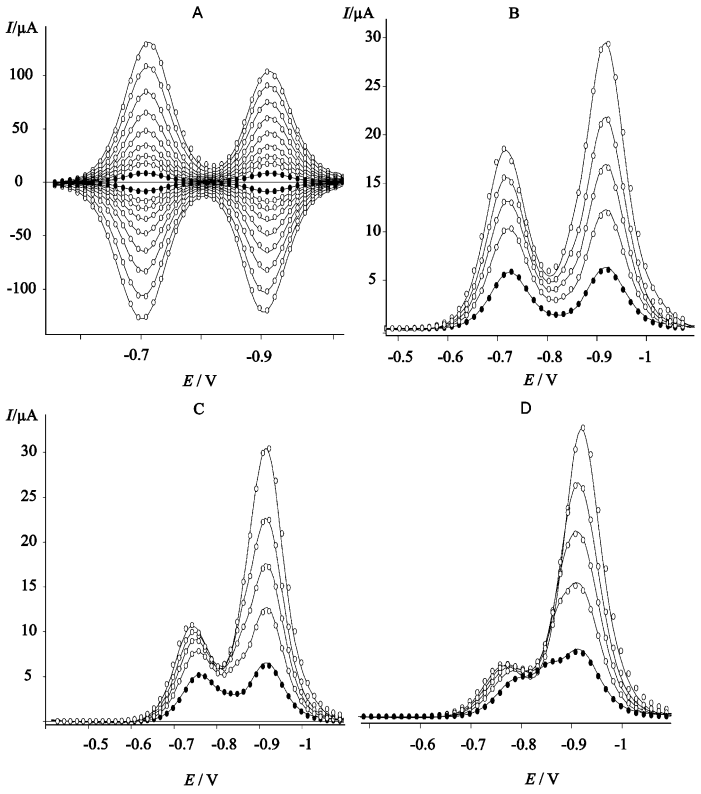

Figure 7. Comparison of measured (——) and calculated (○ ○ ○ ○ ○) square-wave (SW) voltammograms of *trans/cis*-$[Ir(tropp^{Ph})_2]^+$ (*trans/cis*-**1**-Ir): A) SW voltammograms in CH_2Cl_2 showing forward and backward scans at square-wave frequencies of 12, 50, 100, 200, 400, 800, 1500, 3000 and 4800 Hz; B) SW voltammograms in CH_2Cl_2 containing 0.0375 mol L^{-1} acetonitrile; C) SW voltammograms in CH_2Cl_2 containing 0.17 mol L^{-1} acetonitrile; and D) SW voltammograms in CH_2Cl_2 containing 0.73 mol L^{-1} acetonitrile. The square-wave frequencies in B)–D) were 25, 100, 200, 350 and 700 Hz. The curve obtained with the lowest frequency is indicated as (● ● ● ●).

Finally, we refer briefly to the irreversible process (EC mechanism) given in Equation (11) in Scheme 3. Although our experiments do not allow the determination of any exact data, the good fit of the square-wave simulations indicate that any 19-electron neutral complex $[Ir(acn)(tropp^{Ph})_2]^0$ (**9**-Ir) eventually formed must be very unstable, that is, the interaction of the paramagnetic complexes *trans/cis*-$[Ir(tropp^{Ph})_2]^0$ (**2**-Ir) with acn is very slow or the dissociation of **9**-Ir is fast ($k_d \gg 10^4\ s^{-1}$).

Conclusion

The tropp ligand system is very rigid[39] (the only flexible groups are the P-bonded phenyl rings) and, in particular, the rotation of the coordinated olefinic units is blocked. The olefinic NMR resonances can thus be used to readily distinguish between organometallic species in which these protons are related by mirror symmetry and those in which this mirror symmetry is broken. In this work, we used this property to investigate the formation of 18-electron five-coordinate $[ML(tropp^{Ph})_2]$ complexes by reaction of small simple donors (Cl^- or acetonitrile) with four-coordinate 16-electron complexes *trans/cis*-$[M(tropp^{Ph})_2]^+$. These results were helpful in elucidating some important thermodynamic and kinetic relationships between iridium tropp complexes with 16-, 17-, and 18-valence-electron configurations. The following conclusions can be drawn:

1) Small donors react rapidly with the four-coordinate 16-electron complexes *trans/cis*-$[M(tropp^{Ph})_2]^+$ (**1**-M; M = Rh, Ir) to give five-coordinate 18-electron complexes. The second-order rate constants for the formation of the chloro complexes $[MCl(tropp^{Ph})_2]$ (**7**-M; M = Rh, Ir) from the *trans* isomers of the $[M(tropp^{Ph})_2]^+$ ions are slightly faster for rhodium ($k_f \approx 8\times10^5\ M^{-1}\ s^{-1}$) than for iridium ($1\times10^5\ M^{-1}\ s^{-1}$).[40] The formation of the acetonitrile complexes $[M(acn)(tropp^{Ph})_2]^+$ is even faster and could only be estimated for **6**-Ir ($k_f \approx 3\times10^6\ M^{-1}\ s^{-1}$). The significantly larger rates for the formation and dissociation of the corresponding rhodium complexes impeded their observation by electrochemical methods under our conditions. The *cis*-$[M(tropp^{Ph})_2]^+$ complexes react significantly slower than the *trans* isomers; this was demonstrated for the rhodium–tropp complexes. This finding is in agreement with our previous assumption that the *cis* isomers are sterically more congested, which also causes stronger structural distortions. As expected, the five-coordinate iridium complexes are considerably more stable than the rhodium analogues, that is, the first-order dissociation rate constant k_d is at least two orders of magnitude smaller for the chloro complexes $[MCl(tropp^{Ph})_2]$ for M = Ir ($k_d \approx 8\ s^{-1}$) than for M = Rh ($k_d > 2\times10^2\ s^{-1}$). The acetonitrile complexes $[M(acn)(tropp^{Ph})_2]^+$ are significantly more labile; this was specifically shown for $[Ir(acn)(tropp^{Ph})_2]^+$ (**6**-Ir), which dissociates three orders of magnitude faster ($k_d > 3.7\times10^3\ s^{-1}$) than the corresponding chloro complex **7**-Ir. The analyses of the DNMR of the compounds $[MCl(tropp^{Ph})_2]$ hints at the formation of close ion pairs as first intermediates on the dissociation pathways. Ion pairs are increasingly recognized as being important intermediates in many organometallic transformations.[41] Although our findings are very preliminary and certainly must await substantiation, they indicate that these are more stable for rhodium than for iridium complexes.[42]
2) The 16-electron complexes *trans/cis*-$[M(tropp^{Ph})_2]^+$ (**1**-M) do not isomerize in a weakly coordinating solvent. The isomerization of the 17-electron species $[M(tropp^{Ph})_2]^0$ (**2**-M), however, turns out to be quite fast ($\approx 1\times10^4\ s^{-1}$), as was demonstrated for M = Ir. This behavior is expected for four-coordinate d^9-configured complexes;[43] however, to our knowledge has been genuinely demonstrated here for the first time. Interestingly, the four-coordinate anionic 18-electron complexes $[M(tropp^{Ph})_2]^-$, with a d^{10} configuration at the metal center, are rigid on the NMR timescale and, in solution, adopt a distorted tetrahedral structure, which is observed in the solid state (see the formula for **3**-Ir in Scheme 3).[1,2,19]
3) Most importantly with respect to the reactivity of 17-electron $[ML_4]$ complexes, the homogeneous electron

transfer between the 16-electron complexes *trans*/*cis*-[Ir(tropp^{Ph})$_2$]$^+$ (**1**-Ir) and 18-electron complexes [Ir(tropp^{Ph})$_2$]$^-$ (**3**-Ir) is fast ($\approx 5\times10^8\,M^{-1}s^{-1}$). It is likely that the close structural resemblance between the [Ir(tropp^{Ph})$_2$]^n complexes in their various oxidation states is the reason for this. Furthermore, the first and second redox potential is only separated by about 270 mV in CH_2Cl_2 as solvent. Consequently the disproportionation of the paramagnetic species [M(tropp^{Ph})$_2$]^0 (**2**-M) into the diamagnetic complexes **1**-M and **3**-M (M = Rh, Ir) proceeds rapidly; this supports the idea that the last are actually involved in the reactions investigated so far. Although this could only be demonstrated for M = Ir ($k_{disp}\approx 1\times10^4\,M^{-1}s^{-1}$), we assume that the properties of the rhodium complexes are not much different. As a consequence of these findings, one must either search for systems where the two redox potentials are widely separated (i.e., $E^{\circ 2}-E^{\circ 1}>-500$ mV) or the homogeneous electron-transfer rate constant k_{homo} is small, in order to unambiguously investigate the reactivity of paramagnetic 17-electron $[ML_4]^0$ complexes. Not unexpectedly, simple donors like acetonitrile are reluctant to interact with [M(tropp^{Ph})$_2$]^0, that is, the resulting 19-electron complexes are unstable.

4) Except for the *cis*/*trans* equilibrium constant for the paramagnetic iridium(**0**) complexes, which could not be obtained with sufficient accuracy by the simulations and was determined by EPR spectroscopy, the given equilibrium and rate constants reported in this paper have been found by fitting the experimental square-wave voltammograms. The independently determined data from NMR and UV-visible techniques were obtained in order to attach further confidence to the values found by the electrochemical methods. As such, the results presented here give another example of how electrochemical techniques may be applied as a very valuable tool for studying fundamental problems in the reactivity of organometallic complexes.[44]

Experimental Section

Materials and solutions: All complexes reported in this work were prepared according to already published procedures.[1,2,20] Temperature-dependent NMR spectroscopic investigations on the five-coordinate complex [RhCl(tropp^{Ph})$_2$] (**7**-Rh) were performed with a 0.1 M solution of **7**-Rh (57.0 mg, 0.051 mmol) in CD_2Cl_2 (0.5 mL, microsyringe). Three independent datasets A–C (temperature range: 313–203 K; T increment: 10 K) were recorded, each with a different amount of (nBu$_4$N)PF$_6$ electrolyte (A: 6.0 mg, 0.031 M; B: 13.0 mg, 0.067 M; C: 20.0 mg, 0.103 M), which was added in solid form to the solution of **7**-Rh in CD_2Cl_2. For the NMR spectroscopic investigations of the corresponding iridium system (**7**-Ir/**6**-Ir) a 0.026 M solution of **7**-Ir (16.0 mg, 0.013 mmol) in CD_2Cl_2/CD_3CN (0.25 mL each, microsyringe) was prepared. NMR spectra were recorded in a temperature range of 323–255 K (T increment: 5 K)

NMR measurements: NMR spectra were recorded using Bruker Avance instruments operating at ^{1}H Larmor frequencies of 500, 400, 300, and 250 MHz, and are referenced to Ξ = 3.16 MHz, 85% H_3PO_4, and TMS for ^{103}Rh, ^{31}P and ^{13}C and ^{1}H, respectively. The temperature was controlled by a Bruker BVT 3000 digital unit and temperatures read from the unit were corrected by substituting the sample tube for one containing a platinum Pt-100 resistor. Magnetization transfer experiments were performed by using the selective inversion-exchange/recovery monitoring scheme according to the literature.[45] Selective inversion of one resonance in the ^{31}P {^{1}H} NMR spectrum was achieved using Gaussian-shaped pulses of 10 ms duration.

Simulation programs: Line-shape simulations were performed with the MEXICO program package,[30] while the CIFIT program package[32] was used for fitting the monitored data of the magnetization transfer experiments. Within experimental error, a constant value was found for the dissociation rate constant, k_d, independent of the concentration of the five-coordinate complexes. This shows that the dissociation was a first-order kinetic process. The second-order formation rate constants, k_f, were calculated using the appropriate equilibrium constants. Eyring plots were analyzed using the Microsoft Excel program. The different kinds of information which are discussed in the main body of the text above were deduced from activation parameters, in particular from the activation energies $\Delta G^{\#}(T)$. In order to allow a meaningful mechanistic discussion it was necessary to make correct assessments of the error limits of the respective parameters. These limits depended on the errors in the primary data, that is, the rate constants and temperatures. We obtained the variance and relative error in $\Delta G^{\#}$ as a function of the errors in k and T by applying the following equation [Eq. (12)][33] to our data:

$$\frac{\Delta\Delta G}{\Delta G}=\frac{\left\{\left[\frac{\Delta T}{T}\left(\ln\frac{k_B T}{hk}+1\right)\right]^2+\left(\frac{\Delta k^2}{k}\right\}^{1/2}\right.}{\ln\left(\frac{k_B T}{hk}\right)} \qquad (12)$$

Insertion of reasonable values for ΔT and Δk show that $\Delta G^{\#}$ was not excessively sensitive to errors in the primary variables. Assuming the maximum error in the temperature measurement to be about $\Delta T\cong 1$ K and an error in the simulations to determine the individual rate constants to be approximately $\Delta k\cong 10$ to 20%, the $\Delta G^{\#}$ values for a given dataset were more or less invariant and a significant change occured only in the second fractional part. Therefore all $\Delta G^{\#}$ values are given with the first decimal place.

Electrochemical measurements: Square-wave voltammetric measurements were conducted by a three-electrode technique by means of a home-built computer-controlled instrument based on the PCI MIO-16E1 data acquisition board (National Instruments). The experiments were performed in methylene chloride containing 0.5 M tetra-*n*-butylammonium perchlorate under a blanket of solvent-saturated argon. The ohmic resistance, which had to be compensated for, was determined by measuring the impedance of the system at potentials where the faradaic current was negligibly small. A square-wave signal with an amplitude of 25 mV and potential steps of 5 mV were used in all experiments. The square-wave frequency was varied between 10 and 5000 Hz. Because of the high immunity of the square-wave method towards charging currents, a correction for background currents was not necessary for the frequency range mentioned above.

The reference electrode was an aqueous Ag/AgCl electrode connected to the cell through a Luggin-capillary filled with acetone containing 0.5 M tetra-*n*-butylammonium perchlorate. The potential of this reference system was calibrated by measuring the potential of the ferrocenium/ferrocene couple at the end of each experiment. The working electrode was a hanging mercury drop ($m_{Hg\text{-}drop}\approx 3.9$ mg) produced by the CGME instrument (Bioanalytical Systems, West Lafayette, USA) and a platinum wire served as auxiliary electrode.

The evaluation of thermodynamic and kinetic parameters was done by fitting square-wave voltammograms simulated on the basis of the reactions depicted in Scheme 3 to the experimental ones, assuming that the charge-transfer coefficients α were equal to 0.5 for each charge-transfer reaction. The details of the square-wave simulations have been described in reference [36]. The algorithm was implemented in a particular version of the DigiSim simulation program.[37]

Crystal structure determination: CCDC-215523 (**6**-Rh) and CCDC-154346 (**7**-Ir) contain the supplementary crystallographic data for this paper. These data can be obtained free of charge via www.ccdc.cam.ac.uk/conts/retrieving.html (or from the Cambridge Crystallographic

Data Centre, 12 Union Road, Cambridge CB2 1EZ, UK; fax: (+44) 1223-336-033; or deposit@ccdc.cam.uk).

Acknowledgement

This work was supported by the Swiss National Science Foundation. Dr. F. Breher gratefully acknowledges a grant provided by the Deutsche Forschungsgemeinschaft.

[1] Rh^0: H. Schönberg, S. Boulmaâz, M. Wörle, L. Liesum, A. Schweiger, H. Grützmacher, *Angew. Chem.* **1998**, *110*, 1492; *Angew. Chem. Int. Ed.* **1998**, *37*, 1423.
[2] Ir^0: H. Grützmacher, H. Schönberg, S. Boulmaâz, M. Mlakar, S. Deblon, S. Loss, M. Wörle, *Chem. Commun.* **1998**, 2623.
[3] Ir^0: B. Longato, L. Riello, G. Bandoli, G. Pilloni, *Inorg. Chem.* **1999**, *38*, 2818.
[4] Rh^0: B. Longato, R. Coppo, G. Pilloni, R. Corvaja, A. Toffoletti, G. Bandoli, *J. Organomet. Chem.* **2001**, *637–639*, 710–718.
[5] Rh^0: N. Mézailles, P. Rosa, F. Mathey, P. Le Floch, *Organometallics* **2000**, *19*, 2941.
[6] d^{10}-M fluorophosphine complexes (M = Rh, Ir): $[Rh(PF_3)_4]^-$: T. Kruck, N. Derner, W. Lang, *Z. Naturforsch. Teil B* **1966**, *21*, 1020.
[7] $[Rh(CO)_2(PPh_3)_2]^-$ and $[Ir(CO)_3(PPh_3)]^-$: J. P. Collman, F. D. Vastine, W. R. Roper, *J. Am. Chem. Soc.* **1968**, *90*, 2282, and references therein.
[8] $[Rh(CO)_4]^-$: P. Chini, S. Martinengo, *Inorg. Chim. Acta* **1969**, *3*, 21.
[9] $[Ir(CO)_4]^-$: L. Malatesta, G. Caglio, M. Angoletta, *J. Chem. Soc. Chem. Commun.* **1971**, *10*, 2387 and references therein.
[10] $[Ir(PF_3)_4]^-$: M. A. Bennett, D. J. Patmore, *Inorg. Chem.* **1971**, *10*, 2387.
[11] $[Rh(PF_2NMe_2)_4]^-$: D. A. Clement, J. F. Nixon, *J. Chem. Soc. Dalton Trans.* **1973**, 195.
[12] $[Rh(CO)(triphos)]^-$: G. G. Johnston, M. C. Baird, *J. Organomet. Chem.* **1986**, *314*, C51.
[13] Chemical CO_2 reduction with $[Rh(Ph_2P\text{-}(CH_2)_n\text{-}PPh_2)_2]^-$ ($n = 2, 3$): B. Bogdanoviæ, W. Leitner, Ch. Six, U. Wilczok K. Wittmann, *Angew. Chem.* **1997**, *109*, 518; *Angew. Chem. Int. Ed. Engl.* **1997**, *36*, 500.
[14] Hydroformylation: A. S. Chan, H.-S. Shieh, *Inorg. Chim. Acta* **1994**, *218*, 89 and references therein.
[15] Electrochemical CO_2 reduction with $[MCl(CO)(PPh_3)_2]$ (M = Rh, Ir): A. Szymaszek, F. P. Pruchnik, *J. Organomet. Chem.* **1989**, *376*, 133, and references therein.
[16] C–H bond activation: J. A. Sofranko, R. Eisenberg, J. A. Kampmeier, *J. Am. Chem. Soc.* **1980**, *102*, 1163.
[17] Photochemical H_2O reduction: S. Oishi, *J. Mol. Catal.* **1987**, *39*, 225.
[18] A bimetallic Rh^0–Rh^0 catalyst has been used to generate H_2 from HX: A. F. Heyduk, D. G. Nocera, *Science* **2001**, *293*, 1639.
[19] S. Deblon, L. Liesum, J. Harmer, H. Schönberg, A. Schweiger, H. Grützmacher, *Chem. Eur. J.* **2002**, *8*, 601.
[20] C. Böhler, N. Avarvari, H. Schönberg, M. Wörle, H. Rüegger, H. Grützmacher, *Helv. Chim. Acta* **2001**, *84*, 3127; relevant bond lengths [Å] and angles [°] of **4**: Ir–P1 2.292, Ir–P2 2.288, Ir–Ct1 2.050, Ir–Ct2 2.062, C4–C5 1.441, C4a–C5a 1.448; P1-Ir-P2 172.7, Ct1-Ir-Ct2 131.5.
[21] Photocatalytic cycles that produce H_2 from proton sources including water have been intensively studied; for a review see: E. Amouyal in *Homogeneous Photocatalysis*, Vol II, (Ed.: M. Chanon), Wiley, **1997**, p. 263.
[22] Numerous five-coordinate complexes with rhodium and iridium have been investigated in the past decades. For a compilation of structural data see: A. G. Orpen, L. Brammer, F. H. Allen, O. Kennard, D. G. Watson, R. Taylor, *J. Chem. Soc.* **1989**, S1.
[23] A pure Y-type structure of a ML_5 complex has two angles $>120°$ and one smaller than 120° in the equatorial plane. A T-type structure has two angles at 90° and one angle at 180°. Y/T-forms show aspects of both limiting forms and are unsymmetrical: G. Ujaque, F. Maseras, O. Eisenstein, L. Liable-Sands, A. L. Rheingold, W. Yao, R. H. Crabtree, *New J. Chem.* **1998**, 1493 and ref. [24].
[24] J.-F. Riehl, Y. Jean, O. Eisenstein, M. Péllisier, *Organometallics* **1992**, *11*, 729 and references therein.
[25] Due to electronic reasons, five-coordinate complexes with d^6-valence-electron-configured metal centers distort to a Y-structure: H. Werner, A. Hohn, M. Dziallas, *Angew. Chem.* **1986**, 98, 1112; *Angew. Chem. Int. Ed. Engl.* **1986**, *25*, 1090.
[26] This behavior is expected because the thermal interconversion of a square-planar d^8-metal complex is spin-forbidden.
[27] At low temperatures ($T = 233$ K), the complex cation $[Ir(thf)(tropp^{Ph})_2]^+$ gives sharp signals: $\delta(^{31}P) = 53.71$ ppm; C*H*=C*H*$_{trop}$: $\delta(^1H) = 4.27, 4.10$ ppm. Note, however, that although the formation of five-coordinate complexes from *cis*-**1**-Rh with acetonitrile and from *cis*-**1**-Ir with THF is not detected, these isomers must be involved in the equilibrium reaction shown in Scheme 2, as the ratio of *trans* to *cis* isomers remains constant at all temperatures.
[28] For *trans*-$[M(tropp^{ph})_2]^+$ (M = Rh, Ir), structures with $\varphi = 0$–30° have been determined (ref. [1,2] and S. Deblon, H. Schönberg, S. Loss, H. Grützmacher, unpublished results), depending on the counteranion (the intersection angle φ is defined by the planes through P, Rh and the centroid of the C=C bond). We did not succeed in determining the structures of the *cis* isomers of **1**-Rh and **1**-Ir, but their presence in the solid state in amounts corresponding to the isomer ratio in solution (about 20% for M = Rh and 10% for M = Ir) is clearly evident from solid-state CP/MAS-^{31}P NMR (H. Rüegger, unpublished results). Note that the related *cis*-$[Rh(^{Me}tropp^{ph})_2]^+$, carrying methyl groups at the C=C$_{trop}$ unit, shows a severe distortion of $\varphi = 42°$, see ref. [28]. We assume, however, that the $tropp^{Ph}$ ligands swing against each other, without effecting a full rotation which would also equilibrate the *trans* and *cis* isomers, so that the olefinic ^{1}H and ^{13}C signals become equivalent
[29] S. Deblon, H. Rüegger, H. Schönberg, S. Loss, V. Gramlich, H. Grützmacher, *New J. Chem.* **2001**, *23*, 83.
[30] The MEXICO program package was used for the simulations and data evaluation. See: A. D. Bain, G. J. Duns, *Can. J. Chem.* **1996**, *74*, 819; see also: http://www.chemistry.mcmaster.ca/faculty/bain/exchange.html.
[31] a) S. Forsén, R. A. Hoffman, *J. Chem. Phys.* **1963**, *39*, 2892; b) R. A. Hoffman, S. Forsén, *Prog. Nucl. Magn. Reson. Spectrosc.* **1966**, *1*, 15.
[32] The CIFIT program package was used for the simulations and data evaluation. See, a) A. D. Bain, J. A. Cramer, *J. Magn. Reson. Ser. A* **1996**, *118*, 21; b) D. R. Muhandiram, R. E. D. McClung, *J. Magn. Reson.* **1987**, *71*, 187.
[33] J. Sandström, *Dynamic NMR Spectroscopy*, Academic Press, London, **1982**.
[34] The formation of close ion pairs can generally be assumed and is strongly favored when ions interact in media of low permittivity. See: R. B. Jordan, *Reaction Mechanisms of Inorganic and Organometallic Systems*, Oxford University press, **1991**.
[35] J. Orsini, W. E. Geiger, *Organometallics* **1999**, *18*, 1854.
[36] M. Rudolph, S. W. Feldberg, *DigiSim 3.0 Software* **2001**, Bioanalytical Systems, West Lafayette, IN 47906.
[37] M. Rudolph, *J. Electroanal. Chem.* **2001**, *503*, 15.
[38] A. J. Kunin, E. J. Nanni, R. Eisenberg, *Inorg. Chem.* **1985**, *24*, 1852.
[39] J. Thomaier, S. Boulmaâz, H. Schönberg, H. Rüegger, A. Currao, H. Grützmacher, H. Hillebrecht, H. Pritzkow, *New J. Chem.* **1998**, *21*, 947.
[40] The second-order formation rate constants for reactions in Equations (2) and (5) were estimated according to $k_f = k_d/K_d$, with the data for the first-order dissociation constants k_d listed in Table 4 and the equilibrium constants K_d given in Table 3 for M = Rh or, as discussed in the text, for M = Ir ($K_d = K_{(5)} = 5.8 \times 10^{-5}$ M).
[41] a) D. Drago, P. S. Pregosin, A. Pfaltz, *Chem. Commun.* **2002**, 286–287; b) For a very recent work describing the influence of close ion pairs on the heterolytic H_2 cleavage, see K. Gruet, E. Clot, O. Eisenstein, D. Heon Lee, B. Patel, A. Macchioni, R. H. Crabtree, *New J. Chem.* **2003**, 80–87.
[42] As mentioned, a process having a $\Delta G^{\#}$ of about 6 kJ mol^{-1} lower than the one leading to complete dissociation is found for the equilibration of the CH=CH$_{trop}$ protons in $[RhCl(tropp^{Ph})_2]$, which is ascribed to the formation of a close ion pair. On the other hand, if

close ion pairs are formed in the dissociation of $[IrCl(tropp^{Ph})_2]$, the barrier for complete dissociation is much smaller (a difference of $\Delta(\Delta G^{\#}) \approx 1\ kJ\,mol^{-1}$ is obtained as the difference between the activation energies of processes in Equations (4) and (5), see Table 4).

[43] *trans*/*cis*-Isomerization is a thermally forbidden process in square planar complexes with a d^8 configuration at the metal center but becomes allowed in d^9 species: T. A. Albright, J. K. Burdett, M.-H. Whangbo, *Orbital Interactions in Chemistry*, Wiley, New York, **1984**, p. 304.

[44] There are many examples described in the literature in which mechanistic problems in organometallic chemistry have been successfully tackled by electrochemical methods. Only a very restricted number of reviews can be given here: a) D. Astruc, *Electron Transfer and Radical Processes in Transition Metal Chemistry*, VCH, Weinheim, **1995**; b) S. M. Hubig, J. K. Kochi, *Electron Transfer Chem.* **2001**, *2*, 681; c) C. Amatore, A. Jutland, *Acc. Chem. Res.* **2000**, *33*, 314; d) C. Amatore, A. Jutland, *J. Organomet. Chem.* **1999**, *576*, 254; e) W. C. Trogler, *J. Organomet. Chem. Libr.* **1990**, *22*, 306; f) W. C. Trogler, *Int. J. Chem. Kinet.* **1987**, *19*, 1025.

[45] J. J. Led, H. Gesmar, *J. Magn. Reson.* **1982**, *49*, 444 – 463.

Received: May 8, 2003
Revised: July 25, 2003 [F5116]

